Journal of Power Sources 196 (2011) 5070–5076

Contents lists available at ScienceDirect

Journal of Power Sources

journal homepage: www.elsevier.com/locate/jpowsour

Numerical analysis of the effect of different gas feeding modes in a proton exchange membrane fuel cell with serpentine flow-field

J.M. Sierra [a], J. Moreira [b], P.J. Sebastian [a,*]

[a] Centro de Investigación en Energía. Universidad Nacional Autónoma de México, Temixco, Morelos 62580, Mexico
[b] Universidad de Ciencia y Arte de Chiapas, Tuxtla Gutierrez, Chiapas 29000, Mexico

ARTICLE INFO

Article history:
Received 22 December 2010
Accepted 20 January 2011
Available online 28 January 2011

Key words:
Fuel cell
Simulation
Hydrogen
Oxygen
Bipolar plate

ABSTRACT

In this work we present a 3D computational model of a proton exchange membrane fuel cell (PEMFC) to investigate the effect of employing different modes of gas feeding on distributions. The model is based on a commercial fuel cell with serpentine flow-field. From a rigorous analysis of species concentration, current density and ionic conductivity distributions a correct form of feeding gases in the fuel cell is determined. Optimal operating conditions are found for a better utilization of fuel. Simulation results reveal that local current distribution on catalyst layer can be improved by feeding gases in similar mode and changing the channel height. However, polarization curves present an opposite response to this result. The polarization curve obtained in simulation is well correlated with experimental data.

1. Introduction

Fuel cells are electrochemical devices that convert the chemical energy of hydrogen directly into electricity. Their high efficiency and low pollution levels have promoted their use for supplying energy to the next generation electric vehicles. Their modular design and scalability make them excellent candidates for a variety of applications. The main disadvantages for the massive commercialization are the lack of infrastructure and the high production cost. The design optimization is an important issue that can help to reduce their production cost. However, the design optimization requires a good level of knowledge related to the basic processes that take place in PEMFCs [1,2]. With the advances in computational system simulation, an important mathematical tool, it has been helpful to understand the phenomena occurring in the active components of the fuel cell which are difficult to obtain by experimental studies [3].

Mass transport is one of the most important processes that take place inside the PEM fuel cell due to its direct relation with the electrochemical reactions that occur on its electrodes [4,5]. Bipolar plates are the main components on which mass transport depends, because they help to distribute the gas on the catalyst layers. However, different forms of distributing the gases exist and those are by channel configurations [6–9]. Serpentine channel configuration is the widely used one in commercial cells [10,11] and there are many types; some of them with a single channel and others with three or more channels in parallel form [12,13]. This work is focused on the commercial fuel cell (EFC05-01SP) with a three parallel channel design (Fig. 1). The effect of species concentration and ionic conductivity on the distributions was studied. Also, the model was evaluated under different operating conditions; gases were injected in four modes to know the impact of these parameters on the transfer current distributions. Finally, modifications in channel height were done to improve the transfer current distributions on the catalyst layers.

Different modes of gas feeding in fuel cells are shown in Fig. 2: the first case (a) is the feeding mode of *Electrochem* commercial fuel cell; flow-fields are designed to be in a “cross-flow” position, the cathode is placed over the anode and gas feeding is located at the bottom and the exit on the top. The second case (b) is for the same design but hydrogen and oxygen are fed from the opposite sides “Non-symmetrical flows”. The third case (c) “similar flows” is when flow-fields are engraved symmetrically, both hydrogen and oxygen follow in the same flow path direction. Finally, the fourth case (d) is for “counter-flows”, hydrogen and oxygen flow completely in counter-flow directions.

The second analysis realized in this work was to modify the design of the commercial fuel cell, this design has zones where channels have more depth; its effect was compared with a normal design of serpentine flat. Thus, a reduction in channel height was made to see the effect on species and transfer current distributions.

* Corresponding author. Tel.: +52 55 56229841; fax: +52 55 56229742.
E-mail address: sjp@cie.unam.mx (P.J. Sebastian).

0378-7753/$ – see front matter © 2011 Elsevier B.V. All rights reserved.
doi:10.1016/j.jpowsour.2011.01.079

Fig. 1. Experimental monopolar plate (EFC05-01SP) with serpentine flow-field.

Table 1
Model dimensions.

Parameter	Unit	Value
Channel height	mm	0.8
Channel width	mm	0.8
Rib width	mm	0.8
Chamber height	mm	0.8
Cell active area	$(mm)^2$	500
Gas diffusion layer thickness	mm	0.33
Catalyst layer thickness	mm	0.0015
Membrane thickness	mm	0.178

2. Model development

The 3D computational model consists of a single cell fuel cell with serpentine channels, including gas diffusion layers (GDLs), catalyst layers (CLs) and membrane (MEM). The model was built in Gambit® 2.4.6 pre-processor. Dimensions and geometry of the model are shown in Table 1 and Fig. 3, respectively.

In order to establish the accuracy of results and reducing the time of calculations an independent grid analysis was performed. The total number of hexahedral elements (Fig. 3) in the model was 526,160, with a grid size of 0.2 for channels and ribs, 0.05 for gas diffusion layers, 0.004 for catalyst layers and 0.03 for membrane.

Consecutively to solve the model, it was considered the following assumptions: (i) the fuel cell operates under steady-state and non-isothermal conditions; (ii) a laminar flow was considered in the channels, based on Reynolds number calculation; (iii) the porous zone was assumed to be isotropic; (iv) liquid water transport, proton transport, energy and water diluted in the membrane are included in the model; (v) the reaction takes place on the surface of both catalyst layers, and it was assumed that the diffusive flux of the reacting species was balanced electrochemically by production/consumption rate, according to the half-cell reactions.

The model includes the species transport in gas form, proton transport, energy and water diluted in the membrane. The water transport is based on the electro-osmotic and diffusion mechanisms.

2.1. Mathematical model

The governing equations considered for the numerical simulation of the fuel cell were the standard equations of fluid mechanics (conservation of mass, momentum, species transport and energy equations).

The three-dimensional steady state mass conservation equation in the vectorial form is given by:

$$\nabla \cdot (\rho \vec{v}) = S_m \tag{1}$$

where ρ is the density of the mixture, $\vec{v}$ the velocity vector and S_m is a source term that includes the species (S_{H_2}, S_{O_2} and S_{H_2O}) considered in each electrode side.

The momentum conservation equation for a Newtonian fluid is:

$$\nabla \cdot (\rho \vec{v}\vec{v}) = -\nabla p + \nabla \cdot (\mu^{\text{eff}} \nabla \vec{v}) + S_p \tag{2}$$

where ρ is the fluid density, p is the pressure, μ^{eff} is the effective dynamic viscosity and S_p is the source term that includes the porous media properties (Darcy Law).

The species conservation equation is represented by:

$$\nabla \cdot (\rho \vec{v} y_i) = -\nabla \cdot \vec{J}_i + S_i \tag{3}$$

where $\vec{J}_i$ is the species diffusion (laminar flow) and S_i is the source term for the consumption/production rate of each phase.

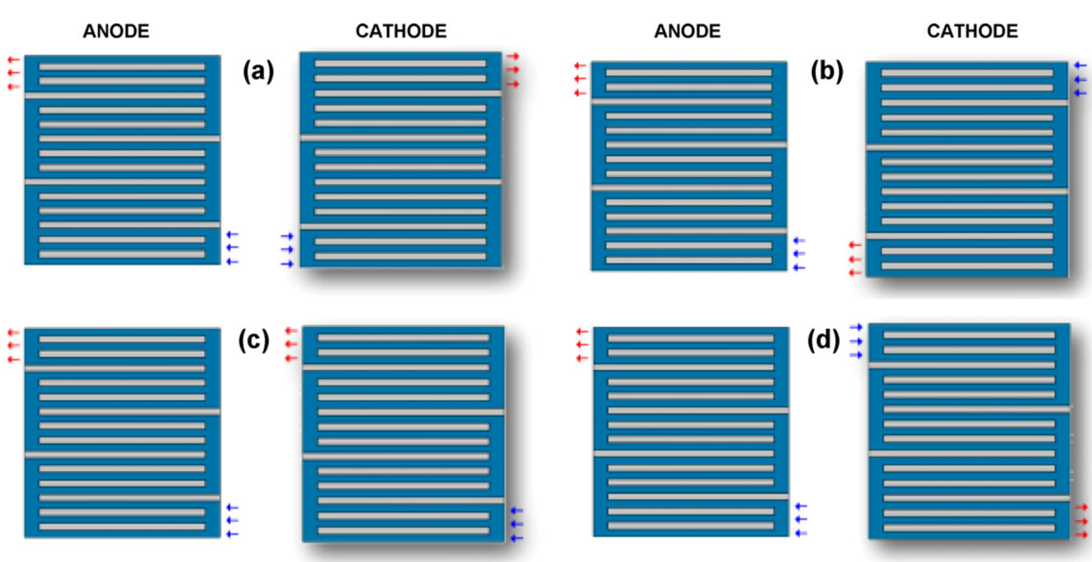

Fig. 2. Different modes of gas feeding in a serpentine design (a) cross-flow, (b) non-symmetrical flow, (c) similar flow, (d) counter flow.

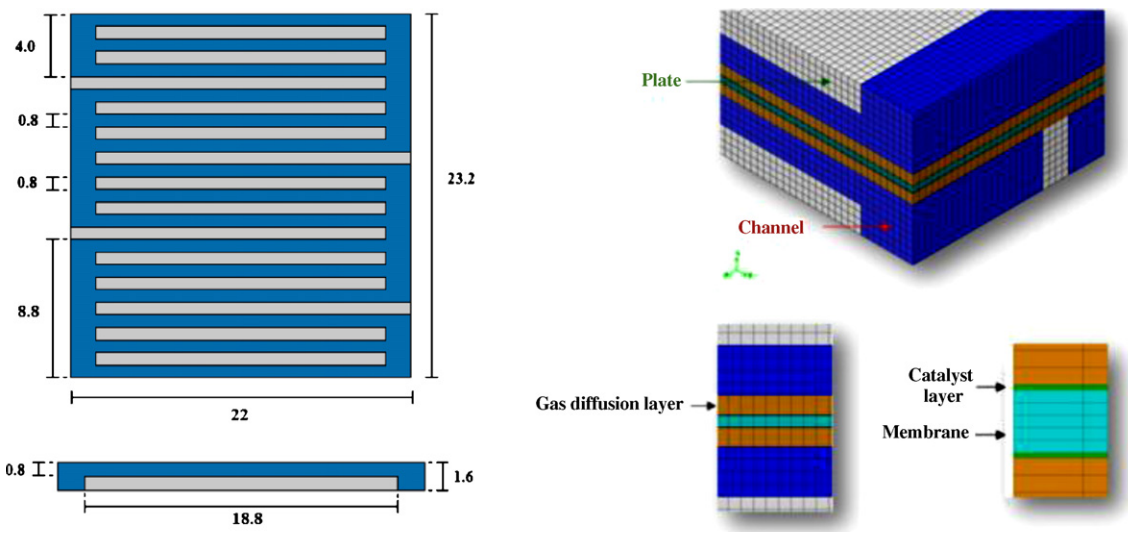

Fig. 3. Flow-field dimensions (mm) and mesh visualization in sub-domains.

The energy conservation equation derived from the first law of thermodynamics is described by:

$$\nabla \cdot (\vec{v}(\rho E + p)) = \nabla \cdot \left(k_{\text{eff}} \nabla T - \sum_j h_j \vec{J}_j \right) + S_h \quad (4)$$

where E is the total energy, k_{eff} is the effective conductivity, and $\vec{J}_j$ is the flux diffusion of species j and h is the enthalpy. S_h is the source term that includes the irreversible processes of heat generation that takes place inside the fuel cell. The two terms on the right-hand side represent the energy transfer due to conduction and species diffusion, respectively. According to different sub-domains used in the model some source terms were added in the equations.

Previous equations were coupled to the electrochemical model which consisted of two potential equations: one potential (Eq. (5)) associated with the electron transport in the catalyst layers, the diffusion layers and the current collectors:

$$\nabla \cdot (\sigma_{\text{sol}} \nabla \phi_{\text{sol}}) + R_{\text{sol}} = 0 \quad (5)$$

where σ_{sol} is the electrical conductivity ($\Omega^{-1}\,\text{m}^{-1}$), ϕ_{sol} is the electrical potential (volts) and R_{sol} is the volumetric transfer current ($\text{A}\,\text{m}^{-3}$), all in the solid phase.

The potential equation (Eq. (6)) associated with the protonic transport, is solved in the membrane and catalyst layers according to:

$$\nabla \cdot (\sigma_{\text{mem}} \nabla \phi_{\text{mem}}) + R_{\text{mem}} = 0 \quad (6)$$

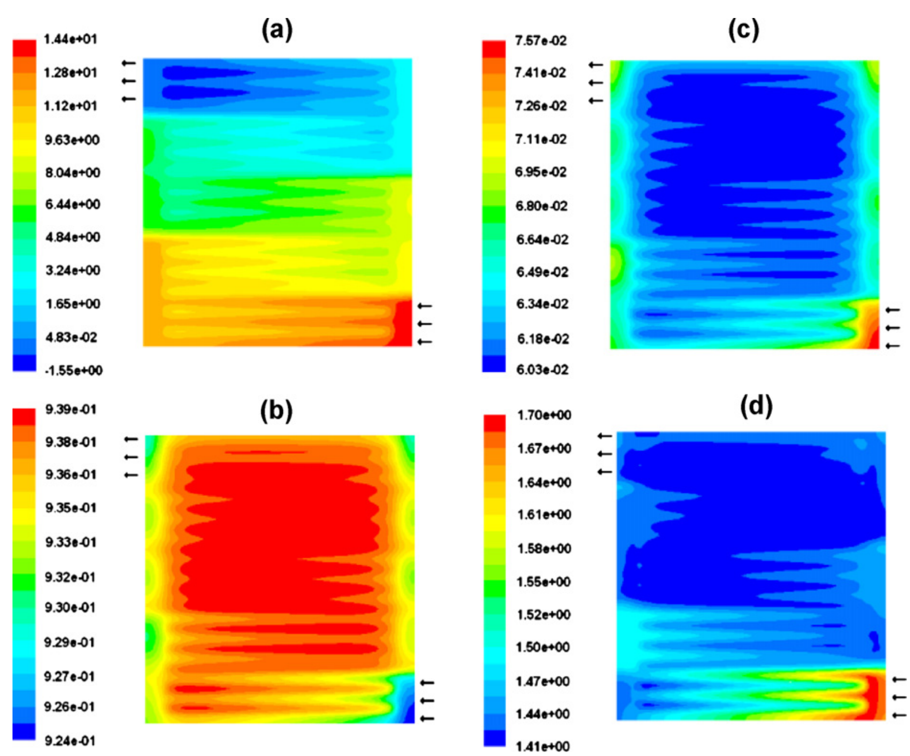

Fig. 4. Local distributions on GDL/CL anode interface, (a) static pressure (Pa), (b) H_2 mass fraction, (c) H_2O mass fraction and (d) protonic conductivity on CL/MEM interface ($\Omega^{-1}\,\text{m}^{-1}$), 0.6 V, 1 atm, 25 °C and 100% RH.

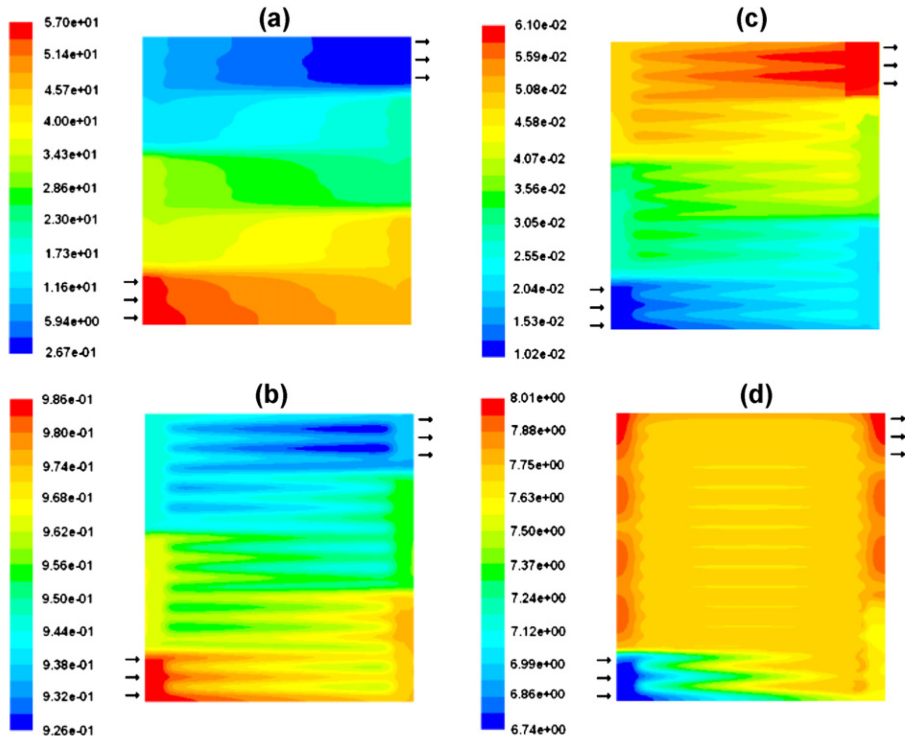

Fig. 5. Local distributions on GDL/CL cathode interface, (a) static pressure (Pa), (b) O_2 mass fraction, (c) H_2O mass fraction and (d) protonic conductivity at CL/MEM interface ($\Omega^{-1}\,m^{-1}$), 0.6 V, 1 atm, 25 °C and 100% RH.

where σ_{mem} is the protonic conductivity, ϕ_{mem} the protonic potential and R_{mem} the volumetric transfer current ($A\,m^{-3}$), all in the membrane phase.

The transfer currents, or the source terms in Eqs. (5) and (6), are non-zero only inside the catalyst layers and are computed as:

- For the solid phase, $R_{sol} = -R_{an}$ (<0) on the anode side and $R_{sol} = +R_{cat}$ (>0) on the cathode side.
- For the membrane phase, $R_{mem} = +R$ (>0) on the anode side and $R_{mem} = -R_{cat}$ (<0) on the cathode side.

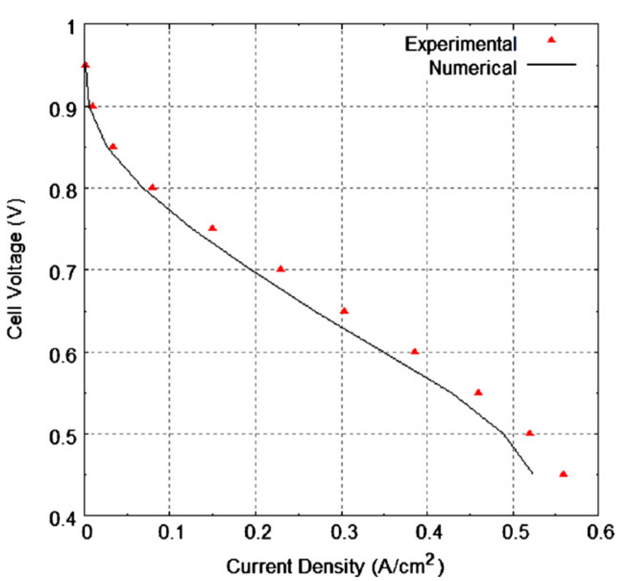

Fig. 6. Experimental and numerical polarization curves for the commercial fuel cell.

The source terms in Eqs. (5) and (6) have the following general definitions:

$$R_{an} = j_{an}^{ref}\left(\frac{[H_2]}{[H_2]_{ref}}\right)^{\gamma_{an}}(e^{\alpha_{an}F\eta_{an}/RT}) \tag{7}$$

$$R_{cat} = j_{cat}^{ref}\left(\frac{[O_2]}{[O_2]_{ref}}\right)^{\gamma_{cat}}(e^{-\alpha_{cat}F\eta_{cat}/RT}) \tag{8}$$

where j^{ref} is the volumetric reference exchange current density in ($A\,m^{-3}$), $[H_2]$ and $[H_2]_{ref}$ are the local species concentration in ($kg\,mol\,m^{-3}$), γ is the concentration dependence (dimensionless), α is the transfer coefficient (dimensionless), η is the activation losses defined in (Eqs. (9) and (10)). F is the Faraday constant ($9.65 \times 10^7\,C\,kg^{-1}\,mol^{-1}$). Subscript (an) corresponds to anode side and subscript (cat) corresponds to cathode side in all cases.

The above equations are the general formulation of the Butler–Volmer function and are used to calculate the transfer current in catalyst layers.

The driving force for the kinetics is the local surface overpotential, η, as the activation losses. It is associated with the difference between the solid and membrane potentials, ϕ_{sol} and ϕ_{mem}.

$$\eta_{an} = \phi_{sol} - \phi_{mem} \tag{9}$$

$$\eta_{cat} = \phi_{sol} - \phi_{mem} - V_{OC} \tag{10}$$

where ϕ_{sol} in Eqs. (9) and (10) is the half-cell potential, which is an input parameter used in the model to specify the operating point of the cell. ϕ_{mem} is the membrane potential and V_{OC} is the open circuit voltage. The electrolyte membrane is modeled as a porous fluid zone. Properties such as ionic conductivity, σ_{mem} and the electro-osmotic drag coefficient are evaluated as functions of the water content λ. These properties are represented by correlations

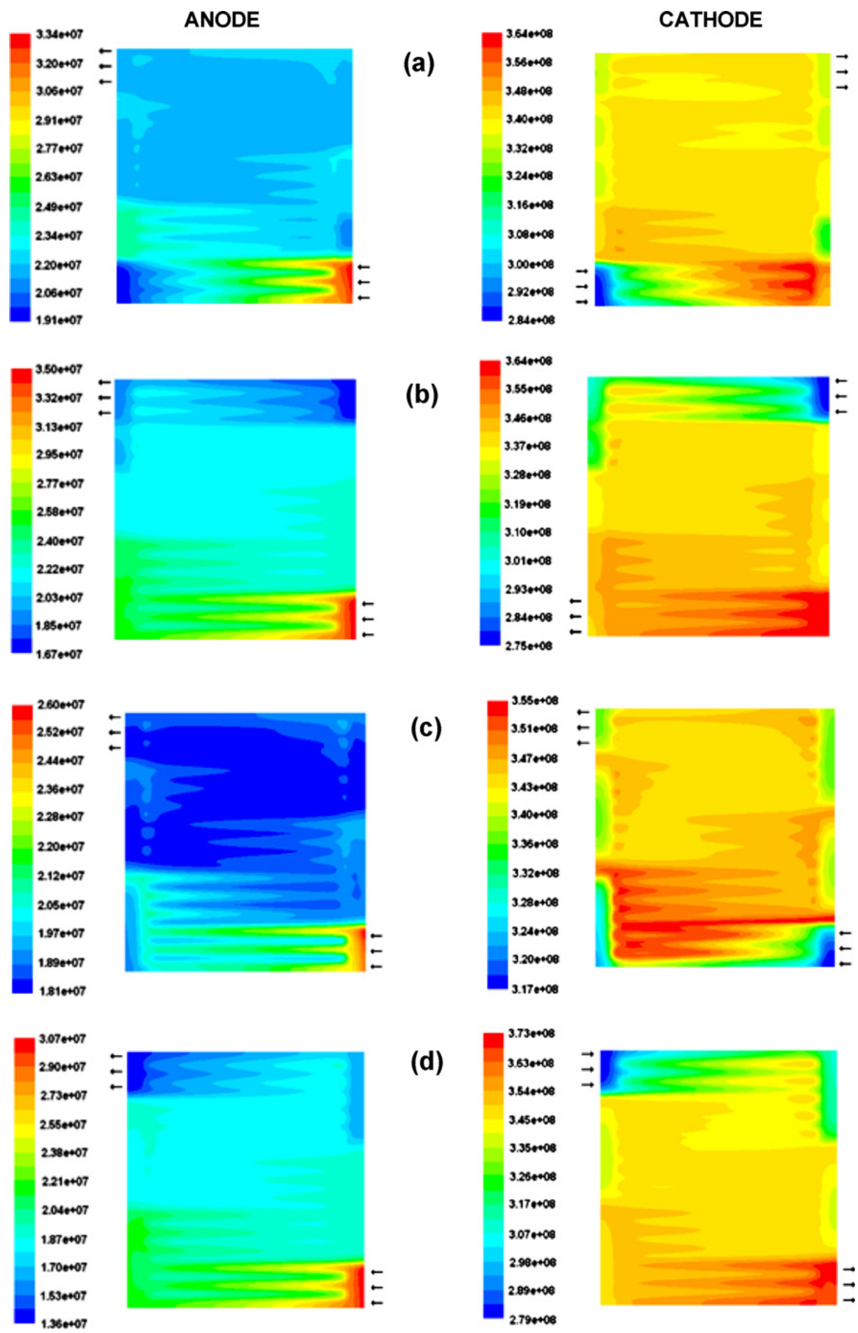

Fig. 7. Transfer current distributions (A m^{-3}) for different modes of gas feeding in the commercial fuel cell, (a) cross-flows, (b) non-symmetrical flows, (c) similar flows, and (d) counter-flows.

suggested by Springer et al. [14] (Eqs. (11) and (12)).

$$\sigma_{mem} = (0.00514\lambda - 0.00326)\, e^{1268((1/303)-(1/T))} \quad (11)$$

$$\lambda = 0.043 + 17.81a - 39.84a^2 + 36a^3 \quad (a < 1)$$

$$\lambda = 14 + 1.4(a - 1) \quad (a > 1) \quad (12)$$

A saturation model reported by Nguyen [15] and Nam et al. [16] is used to simulate the formation and transport of liquid water inside the PEM fuel cell.

From Eq. (5) through Eq. (12) and from other correlations the two potential fields were obtained and they correspond to the three main electrochemical processes that take place in a fuel cell: activation losses, ohmic resistance and concentration losses. The equations were solved using a segregated solver, a first order scheme and the SIMPLE algorithm.

2.2. Modeling parameters

It was important to choose the appropriate parameters for modeling the processes occurring in PEM fuel cells. Operating conditions and electrochemical parameters were taken from experimental values and literature data, respectively. These parameters are showed in (Table 2). The electrochemical parameters were used in Eqs. (7) and (8) to calculate the transfer current in catalyst layers.

2.3. Boundary conditions

"Mass flow inlet" for anode and cathode was set as boundary condition at inlet channels. The anode mass flow was

Table 2
Physical and electrochemical parameters.

Parameter	Symbol	Unit	Value
Anode pressure	P_{an}	atm	1
Cathode pressure	P_{ca}	atm	1
Cell temperature (H_2)	T_C	K	300
Fuel and oxidant temperature (H_2, O_2)	T_i	K	300
Relative humidity (H_2)	–	%	100
Relative humidity (O_2)	–	%	100
Reference exchange current density (anode)	j_{an}^{ref}	$A\,m^{-3}$	1×10^9
Reference exchange current density (cathode)	j_{cat}^{ref}	$A\,m^{-3}$	2.7×10^6
Anode transfer coefficient	α_{an}	–	0.8
Cathode transfer coefficient	α_{cat}	–	0.5
Concentration exponent (anode)	γ_{an}	–	0.5
Concentration exponent (cathode)	γ_{cat}	–	1

$5.94 \times 10^{-8}\,kg\,s^{-1}$ considering a 1.5 stoichiometry and $0.6\,A\,cm^{-2}$ of reference current density. The cathode mass flow at 2.0 stoichiometry was $4.47 \times 10^{-7}\,kg\,s^{-1}$. "Pressure Outlet" was set as boundary condition at outlet channels considering 1 atm of operating pressure. Temperature was fixed at 300 K in external walls of plates and inlet gases.

3. Results and discussion

The results obtained by simulating PEMFC computational model are presented in this section. From basic equations of fluid mechanics and electrochemical models of ANSYS Fluent 12.0 [17] it was possible to investigate the effects of species concentration, transfer current and ionic conductivity distributions in the fuel cell related with different forms of gas feedings. This helped to determine the correct form of injecting gases in the serpentine flow-field.

The computational model was solved in 3D, however to appreciate the simulation results on specific surfaces, interfaces or planes were considered: gas diffusion layer – catalyst layer (GDL/CL) interface and catalyst layer – membrane (CL/MEM) interface.

3.1. Serpentine design

Fig. 4 shows the pressure (a), hydrogen mass fraction (b) and water mass fraction (c) distributions on gas diffusion layer/catalyst layer (GDL/CL) of anode interface. The ionic conductivity (d) on the membrane is shown on catalyst layer/membrane (anode side) interface (CL/MEM). In this figure it is possible to observe that pressure is reduced gradually along the flow-field by adopting the pattern of three parallel channels; hydrogen concentration is high and uniform over the whole surface except at the inlet and some zones where channels have higher depth, the water is absorbed into these areas and their concentration is very low over the entire surface. The protonic conductivity (d) in the membrane presents a similar distribution associated to water concentration and also is low over the surface.

Fig. 5 shows the same type of distributions for cathode side and some different effects can be observed; gas pressure (a) is reduced gradually while the gas advances in the three parallel channels but pressure drop is higher than anode side. This pressure drop is due to oxygen properties and its diffusion through gas diffusion layer. Oxygen concentration distribution (b) adopt a similar pattern, it is high at the inlet and reduces along the channels. Water concentration (c) shows an opposite distribution, it is low at the inlet and high at the outlet due to water generation and water removal in this electrode. Serpentine designs are characterized for the efficient removal of water in gas diffusion layers [7], avoiding the water flooding at high flow velocities. The protonic conductivity (d) on this side is higher than that at the anode side. The water generation on this electrode improves the hydration level of the membrane.

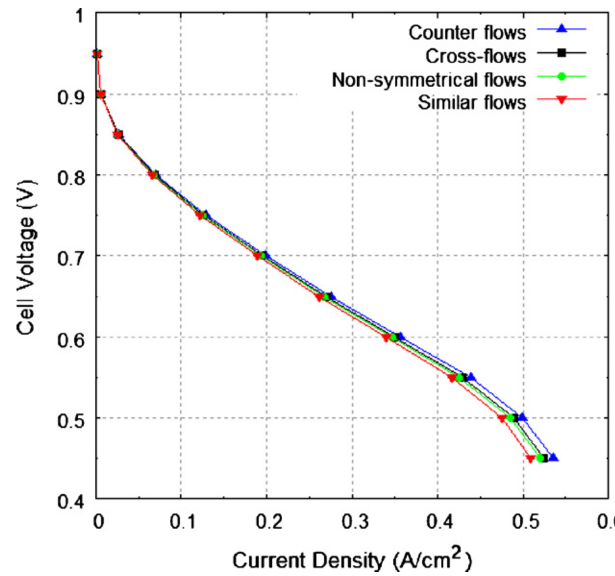

Fig. 8. Experimental and numerical polarization curves for the commercial fuel cell.

Fig. 6 shows the experimental and numerical polarization curves for commercial fuel cell and the computational model. Simulation results and numerical curves were obtained using a workstation Xeon® with 2 dual cores of 2.6 GHz and 2 GB Ram. The CPU time to obtain the numerical curve was about 121 h. The polarization curve is well correlated with the experimental data.

3.2. Study of gas feeding

The previous analysis made it clear that transfer current distributions are closely associated with the protonic conductivity in the membrane and they depend on the gas distributions. The simulation results for four modes of gas feeding in fuel cell are shown in Fig. 7. The results are presented for transfer current contours at 0.6 V. First case (a) is for "cross-flows", second case (b) is for "non-symmetrical flows", third case (c) is for "similar flows" and fourth case (d) is for "counter-flows".

For cross-flows (a) the transfer current on anode side did not show an even distribution along the flow-field, it is too high at the hydrogen inlet and too low at the oxygen inlet. The parameter associated with this distribution was the protonic conductivity distributions in the membrane, Fig. 4(d), which are strongly related to water concentration.

The transfer current distribution on cathode side is similar to the protonic conductivity distribution shown in Fig. 5(d); however, the only parameters associated with the high magnitude of the contours at the inlet of anode channel are the water concentration and protonic conductivity of the anode side, Fig. 4(d). This indicates that the processes that take place in both electrodes are strongly related with each other, trying to reach a mass transfer balance between them.

For non-symmetrical flows, Fig. 7(b), the transfer current distribution on anode side showed high values in the anode inlet channel and low values in the inlet of cathode channel, similar to the water concentration, Fig. 4(c), and protonic conductivity, Fig. 4(d), contours on this electrode. The transfer current distribution on cathode was different to the cross-flows case but the effect of feeding the gas mixture of anode in this location also causes an important contribution. This effect linked to water concentration and protonic conductivity distribution on cathode side causes different transfer current distributions on the electrode.

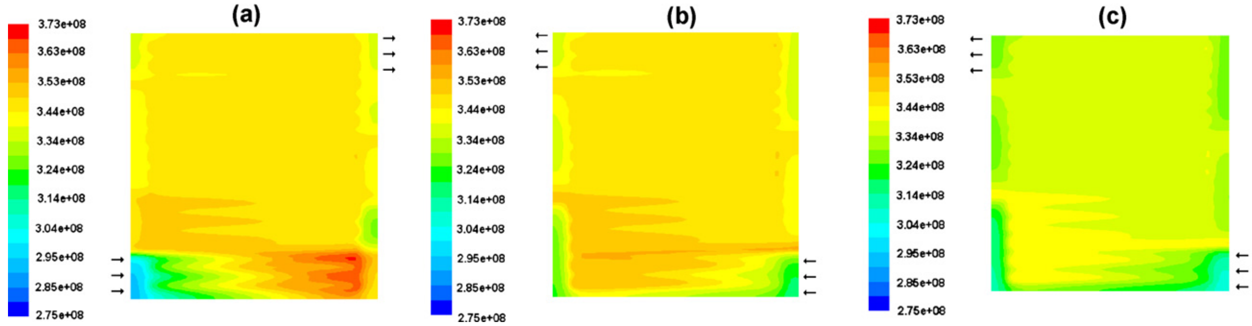

Fig. 9. The transfer current distributions (A m^{-3}) on cathode catalyst layers for (a) commercial design, (b) serpentine-flat "similar-flow" and (c) height reduced "similar-flow".

For similar flows, Fig. 7(c), it is possible to notice that transfer current contours on cathode side showed the best distribution. A more even distribution was observed when gases were injected at the same location. This distribution indicates that processes that take place within the fuel cell are favored when reactions are carried out simultaneously (in the same direction of the flow).

For counter-flows, Fig. 7(d), the transfer current distribution was similar to non-symmetrical flows, but this feeding mode showed the highest value of transfer current (3.73×10^8 A m^{-3}) on the cathode side. It is because, the anode inlet and cathode outlet are located in this section, the water liquid formation improves the hydration level of the electrolyte and thus the protonic conductivity in both sides of the membrane.

Fig. 8 shows the polarization curves for different gas feeding modes of serpentine flow-field. In contrast to contours that showed "similar flows" it is a better form of feeding gas to obtain an even distribution, counter flow feeding presents values slightly higher than other configurations. It can also be observed in the scale of contours in Fig. 7.

3.3. Modified serpentine

In order to distinguish the effect caused by the channel height in the commercial fuel cell, two additional models were evaluated. One of them was a serpentine flat with three channels in parallel and other with the channel height reduced to half. The results are shown in Fig. 9 and it can be observed that transfer current distributions in the commercial design (a) presents a different distribution at hydrogen and oxygen inlets; however, when gases are fed in the same mode and serpentine channels have the same height (b), transfer current distributions are more uniform on the catalyst layer. When serpentine channels are reduced to 0.4 mm (c) the transfer current distribution is more even on the surface than the second case. The scale of the contours was fit in the same value to observe the difference between them.

4. Conclusions

A 3D computational model of PEM fuel cell was developed in this work. The effect of different gas feedings was investigated in the serpentine flow-field. The model was based on the solution of governing equations of fluid dynamics and electrochemical model of Ansys Fluent 12.0. From these equations species concentration and protonic conductivity contours were obtained and helped to explain the transfer current variations in the catalyst layers. The mode of feeding gases that showed the most even transfer current distribution on cathode catalyst layer was "similar-flows". It was possible to determine that processes that take place inside the fuel cell should occur symmetrically to improve the fuel and oxidant utilization in fuel cell as well as the catalytic area. Also, the simulation results showed that channel height for serpentine flow-field should be reduced to improve the mass transport on both the electrodes. However, in the polarization curves the effect is opposite to that in contours, high density current values are obtained when gases were fed at counter-flow mode. In this way a time dependent analysis could demonstrate which form of gas feeding mode results better. Also, it is important to consider the degradation of membrane/electrodes assembly in this issue.

Acknowledgements

This work was financially supported by CONACyT through the project 100212 and DGAPA-UNAM through the project IN103410. J. M. Sierra acknowledges CONACyT for the doctorate scholarship.

References

[1] S. Li, J. Cao, W. Wangard, U. Becker, Proceedings of the 3rd International Conference on Fuel Cell Science Engineering and Technology, Ypsilanti, Michigan, 2005.
[2] S. Um, C.Y. Wang, K.S. Chen, J. Electrochem. Soc. 147 (2000) 4485.
[3] D.H. Jeon, S. Greenway, S. Shimpalee, J.W. Van Zee, Int. J. Hydrogen Energy 33 (2008) 1052.
[4] H. Li, T. Zhou, P. Cheng, J. Heat Transfer 127 (2005) 1363.
[5] T. Berning, N. Djilali, J. Power Sources 124 (2003) 440.
[6] X. Li, I. Sabir, J. Hydrogen Energy 30 (2005) 359.
[7] J. Larminie, A. Dicks, Fuel Cells Systems Explained, 2nd ed., Wiley, 2003.
[8] F. Barbir, PEM Fuel Cells – Theory and Practice, Academic Press, Elsevier, 2005.
[9] F.B. Weng, A. Su, G.B. Jung, Y.C. Chiu, J. Power Sources 143 (2005) 103.
[10] N. Djilali, P.T. Nguyen, T. Berning, J. Power Sources 130 (2004) 149.
[11] S. Shimpalee, J.W. Van Zee, J. Hydrogen Energy 32 (2006) 842.
[12] S. Shimpalee, S. Greenway, J.W. Van Zee, J. Power Sources 160 (2006) 398.
[13] C.H. Huang, J.W. Lin, J. Electrochem. Soc. 156 (2009) B178.
[14] T.E. Springer, T.A. Zawodzinski, S. Gottesfeld, J. Electrochemical Soc. 138 (1991) 2334.
[15] T.V. Nguyen, Tutorial Electrochem. Eng. Math. Model. 14 (1999) 222.
[16] J.H. Nam, M. Kaviany, J. Heat Mass Transfer 46 (2003) 4595.
[17] Fluent 6.3 – Fuel Cells Module Manual, 2007.